6518 *Inorg. Chem.* **2010**, *49*, 6518–6524
DOI: 10.1021/ic100268q

Inorganic Chemistry
Article

Structure Change via Partial Se/Te Substitution: Crystal Structure and Physical Properties of the Telluride $Ba_2Cu_{4-x}Te_5$ in Contrast to the Selenide-Telluride $Ba_2Cu_{4-x}Se_yTe_{5-y}$

Oottil Mayasree, Yanjie Cui, Abdeljalil Assoud, and Holger Kleinke*

Department of Chemistry, University of Waterloo, Waterloo, ON, Canada N2L 3G1

Received February 9, 2010

The chalcogenides $Ba_2Cu_{4-x}Se_yTe_{5-y}$ were synthesized from the elements in stoichiometric ratios at 700 °C, followed by annealing at 600 °C. The ternary telluride $Ba_2Cu_{4-x}Te_5$ crystallizes in a new structure type, space group $C2/c$, with lattice dimensions of $a = 9.4428(6)$ Å, $b = 9.3289(6)$ Å, $c = 13.3028(8)$ Å, $\beta = 101.635(1)°$, $V = 1147.8(1)$ Å^3, for $x = 0.75(1)$ ($Z = 4$). The corresponding selenide-telluride adopts another new, but strongly related, structure type, space group $P4_12_12$, with $a = 6.5418(3)$ Å, $c = 25.782(2)$ Å, $V = 1103.3(1)$ Å^3, for $Ba_2Cu_{3.26(2)}Se_{0.729(8)}Te_{4.271}$ ($Z = 4$). Between 0.13 and 1.0 Te per formula unit can be replaced with Se, while the Cu content appears to vary only within $0.67 \leq x \leq 0.81$ for $Ba_2Cu_{4-x}Se_yTe_{5-y}$. Despite crystallizing in different crystal systems, the telluride and the selenide-telluride exhibit topologically equivalent structure motifs, namely, chains of $Cu(Se,Te)_4$ tetrahedra with a Cu atom cis/trans chain as well as an almost linear Te atom chain. All these chalcogenides, as far as measured, are *p*-doped semiconductors, as determined by Seebeck coefficient and electrical conductivity measurements.

Introduction

Following the encouraging reports about the thermoelectric properties[1−3] of $BaCu_2Te_2$[4] and $A_2BaCu_8Te_{10}$ (A = K, Rb, Cs),[5] we began to systematically investigate the Ba/(Cu, Ag)/(Se,Te) system. Thereby, several new polychalcogenides were discovered, namely, first $Ba_3Cu_{14-x}Te_{12}$ with Te_2^{2-} dumbbells, and very low thermal conductivity,[6] then second $Ba_{6.76}Cu_{2.42}Te_{14}$ with bent Te_3^{2-} units,[7] followed by $Ba_2Ag_4Se_5$ and its Cu-substituted variants with the first linear Se_3^{4-} unit ever found.[8]

Using both selenium and tellurium within one reaction, we succeeded in uncovering another new structure type, adopted by $Ba_3Cu_{17-x}Se_{11-y}Te_y$, which neither exists as a pure selenide nor as a pure telluride.[9] This was another application of the anionic DFSO concept, which has proven to be quite successful in this decade. At its beginning, the DFSO concept[10,11] was employed while designing new sulfides with differential fractional site occupancies on the cation sites, namely, $Nb_{1.72}Ta_{3.28}S_2$,[12] $Nb_{0.95}Ta_{1.05}S$,[13] $Nb_{4.92}Ta_{6.08}S_4$,[14] and $Nb_{6.74}Ta_{5.26}S_4$.[15] More and more examples were found thereafter, with different metal atoms such as Zr and Ti ($Zr_{4.32}Ti_{2.68}Sb_7$[16]), Zr and V ($Zr_{7.5}V_{5.5}Sb_{10}$[17]), Hf and Nb ($Hf_5Nb_5Ni_3P_5$,[18] $Hf_{1.5}Nb_{1.5}As$[19]), and Ti and Ta ($Ti_{1.3}Ta_{9.7}Ge_8$[20]), to name a few. Subsequently, it became apparent that the same concept may be applied to mixed anionic constituents.[21,22] Examples with Se and Te besides $Ba_3Cu_{17-x}Se_{11-y}Te_y$[9] are $Ta_{15}Si_2Se_yTe_{10-y}$[23] and $LnSeTe_2$

*To whom correspondence should be addressed. E-mail: kleinke@uwaterloo.ca.

(1) Tritt, T. M. *Science* **1995**, *272*, 1276–1277.
(2) DiSalvo, F. J. *Science* **1999**, *285*, 703–706.
(3) Rowe, D. M. *Thermoelectrics Handbook: Macro to Nano*; CRC Press, Taylor & Francis Group: Boca Raton, FL, 2006.
(4) Wang, Y. C.; DiSalvo, F. J. *J. Solid State Chem.* **2001**, *156*, 44–50.
(5) Patschke, R.; Zhang, X.; Singh, D.; Schindler, J.; Kannewurf, C. R.; Lowhorn, N.; Tritt, T.; Nolas, G. S.; Kanatzidis, M. G. *Chem. Mater.* **2001**, *13*, 613–621.
(6) Assoud, A.; Thomas, S.; Sutherland, B.; Zhang, H.; Tritt, T. M.; Kleinke, H. *Chem. Mater.* **2006**, *18*, 3866–3872.
(7) Cui, Y.; Assoud, A.; Xu, J.; Kleinke, H. *Inorg. Chem.* **2007**, *46*, 1215–1221.
(8) Assoud, A.; Xu, J.; Kleinke, H. *Inorg. Chem.* **2007**, *46*, 9906–9911.
(9) Kuropatwa, B.; Cui, Y.; Assoud, A.; Kleinke, H. *Chem. Mater.* **2009**, *21*, 88–93.
(10) Yao, X.; Marking, G.; Franzen, H. F. *Ber. Bunsen-Ges.* **1992**, *96*, 1552–1557.
(11) Köckerling, M.; Franzen, H. F. *Croat. Chem. Acta* **1995**, *68*, 709–719.
(12) Yao, X.; Franzen, H. F. *J. Am. Chem. Soc.* **1991**, *113*, 1426–1427.
(13) Yao, X.; Miller, G. J.; Franzen, H. F. *J. Alloys Compd.* **1992**, *183*, 7–17.
(14) Yao, X.; Franzen, H. F. *J. Solid State Chem.* **1990**, *86*, 88–93.
(15) Yao, X.; Franzen, H. F. *Z. Anorg. Allg. Chem.* **1991**, *598−599*, 353–362.
(16) Kleinke, H. *J. Am. Chem. Soc.* **2000**, *122*, 853–860.
(17) Kleinke, H. *Chem. Commun.* **1998**, 2219–2220.
(18) Kleinke, H.; Franzen, H. F. *J. Am. Chem. Soc.* **1997**, *119*, 12824–12830.
(19) Warczok, P.; Chumak, I.; Richter, K. W. *J. Solid State Chem.* **2009**, *182*, 896–904.
(20) Richter, K. W.; Flandorfer, H.; Franzen, H. F. *J. Solid State Chem.* **2002**, *167*, 517–524.
(21) Kleinke, H. *Trends Inorg. Chem.* **2001**, *7*, 135–149.
(22) Kleinke, H. *J. Alloys Compd.* **2002**, *336*, 132–137.
(23) Debus, S.; Harbrecht, B. *Z. Anorg. Allg. Chem.* **2001**, *627*, 431–438.

 Published on Web 06/18/2010

with Ln = lanthanoid.[24] With this contribution, we present the first example, in which incorporating Se into a polytelluride changes the structure while retaining the structure motifs.

Experimental Section

Syntheses and Analyses. All elements were used as acquired: Ba pieces: 99% nominal purity, Sigma Aldrich; Cu powder: 99.9%; Alfa Aesar; Se powder: 99.999%, Sigma Aldrich; Te powder: 99.8%, Sigma Aldrich. The telluride was first found in a (roughly 500 mg) sample starting from Ba, Cu, and Te in the 4:8:13 ratio. The elements were loaded into a silica tube in an argon-filled gloved box, which was then sealed under dynamic vacuum. The fused tube was placed into a resistance furnace, heated to 700 °C within 24 h, and kept at that temperature for 4 days. Such a temperature was expected to achieve a molten sample. To allow for crystallization, the furnace was slowly cooled to 200 °C over a period of 10 days.

After the main product was identified to be $Ba_2Cu_{4-x}Te_5$ (with $x = 0.67$, space group $C2/c$) via a single crystal structure determination described below, we tried to obtain phase pure samples by varying x between 0.5 and 1.0 in steps of 0.1. These mixtures were also heated in fused silica tubes to 700 °C for 2 h, and then at 600 °C for 20 days. To increase homogeneity, the samples were then ground and reheated at 600 °C for another 10 days. This procedure yielded pure samples for $x = 0.7$ and 0.8, but not for the others, as determined utilizing the X-ray powder diffractometer (INEL) with position sensitive detector employing Cu−Kα_1 radiation.

To investigate whether Se atoms may be incorporated into this structure, reactions were carried out with different Se contents, starting from 2 Ba: 3.3 Cu: y Se: $(5-y)$ Te with y = 0.10, 0.25, 0.5, 0.8, 1.0, and 1.5. These reaction mixtures were heated at 570 °C for 5 days, and then slowly (over a period of 4 days) cooled down to room temperature. Thereafter, the reaction mixtures were ground and then reheated at 550 °C for several days. Since all powder diagrams looked distinctly different from the pattern calculated for the $Ba_2Cu_{4-x}Te_5$ model, a single crystal from the sample with $y = 0.8$ was selected for single crystal structure studies. After the successful structure solution, which resulted in the formula $Ba_2Cu_{3.26}Se_{0.73}Te_{4.27}$ and space group $P4_12_12$, the powder diagrams could be identified as containing exclusively the reflections of this new type for $0.25 \le y \le 1.0$, while the more Se-rich and the more Se-poor sample exhibited additional reflections belonging to minor side products including $BaCu_2(Se,Te)_2$ and BaTe, respectively. One can thus conclude that the Se content of tetragonal $Ba_2Cu_{4-x}Se_yTe_{5-y}$ may vary at least within $0.25 \le y \le 1.0$, but does not reach 0.10 or 1.5.

A differential scanning calorimetry (DSC) experiment carried out under a flow of argon on the sample with $y = 0.8$, using a NETZSCH STA 409PC Luxx as described earlier,[25,26] pointed to a melting point of 640 °C, and one with $Ba_2Cu_{3.3}Te_5$ to a melting point of 620 °C.

The samples of nominal compositions $Ba_2Cu_{3.3}Te_5$, $Ba_2Cu_{3.3}Se_{0.8}Te_{4.2}$, and $Ba_2Cu_{3.3}SeTe_4$ were analyzed via energy dispersive analysis of X-rays using an electron microscope (LEO 1530) with an additional EDX device (EDAX Pegasus 1200). The Ba:Cu:Te ratio, averaged over several crystals, was 20.1:31.6:48:3 atomic-% for the ternary telluride, which compares nicely with the numbers calculated from the nominal formula (19.4:32.0:48.6 at-%). In case of $Ba_2Cu_{3.3}Se_{0.8}Te_{4.2}$ (nominal 19.4:32.0:7.8:40.8 at-%), the Ba:Cu:Se:Te ratio was averaged to 18.0:34.9:9.3:37.8 at-%, revealing a significant incorporation of Se.

Table 1. Crystallographic Data for $Ba_2Cu_{4-x}Te_5$

refined formula	$Ba_2Cu_{3.33(1)}Te_5$, I	$Ba_2Cu_{3.25(1)}Te_5$, II	$Ba_2Cu_{3.24(1)}Te_5$, III
formula weight [g/mol]	1124.3	1118.6	1117.9
T of measurement [K]	298(2)	298(2)	298(2)
λ [Å]	0.71073	0.71073	0.71073
space group	$C2/c$	$C2/c$	$C2/c$
a [Å]	9.472(1)	9.4428(6)	9.4425(8)
b [Å]	9.357(1)	9.3289(6)	9.3390(7)
c [Å]	13.304(2)	13.3028(8)	13.316(1)
β [°]	101.688(3)	101.635(1)	101.567(2)
V [Å^3]	1154.7(3)	1147.8(1)	1150.4(2)
Z	4	4	4
μ [mm^{-1}]	25.06	25.05	24.98
ρ_{calcd} [g/cm^3]	6.47	6.47	6.45
$R(F_o)^a \backslash R_w(F_o^2)^b$	0.051\0.076	0.041\0.063	0.043\0.079

$^a R(F_o) = \sum||F_o| - |F_c||/\sum|F_o|$ (all data). $^b R_w(F_o^2) = [\sum w(F_o^2 - F_c^2)^2/\sum w(F_o^2)^2]^{1/2}$ (all data).

Structure Determination. A single crystal of the nominal composition "$Ba_4Cu_8Te_{13}$", crystal I, was selected for the structure determination. Data were collected on the Bruker Smart APEX CCD diffractometer with graphite-monochromatized Mo−Kα_1 radiation, via ω scans of 0.3° in two groups of 606 frames at $\phi = 0°$ and 90°. The crystal was exposed for 60 s to the radiation for each frame. The data were corrected for Lorentz and polarization effects. Absorption corrections were based on fitting a function to the empirical transmission surface as sampled by multiple equivalent measurements using SADABS incorporated into the package SAINT.[27]

The SHELXTL program package[28] was utilized for the structure solution and refinements. On the basis of the lattice parameters, monoclinic C-centered was chosen as the Bravais lattice. The systematic absences restricted the possible space groups to $C2/c$ and Cc. Using the "Direct Methods" of SHELXS yielded one Ba, two Cu, and three Te atoms in the space group $C2/c$. Subsequent refinements revealed large thermal expansion parameters in case of the two Cu sites, most notably so for Cu1, and significantly anisotropic ones in case of two of the three Te sites, with $U_{22} \approx 2\,U_{11} \approx 2\,U_{33}$. Therefore, the occupancy factors of the Cu sites were refined, yielding deficiencies of 31% (Cu1) and 3% (Cu2), respectively, and split sites were introduced for the Te sites, yielding two additional sites with the smaller occupancies, namely, 29% and 33% Te, respectively. Refining the occupancies lowered R1 from 0.082 to 0.067, and introducing the split sites to 0.051 (all data). Studying all measured reflections in reciprocal space, viewed along a^*, b^*, and c^* did not reveal any systematic twinning or an intergrowth crystal. Because no improvements were noticeable in lowering the symmetry to Cc, and no evidence for long-range ordering via super cell formation was found, the space group $C2/c$ remained as the final choice. Finally, all atomic positions were standardized with the TIDY program as included in the PLATON package.[29]

To investigate the existence of a phase range and whether or not the Te split sites occur in all cases, two more crystals were analyzed, one from the nominal composition "$Ba_2Cu_{3.3}Te_5$", crystal II, and one from "$Ba_3Cu_{3.2}Te_5$", crystal III. All three data sets gave comparable results, with refined formulas of $Ba_2Cu_{3.33(1)}Te_5$, $Ba_2Cu_{3.25(1)}Te_5$, and $Ba_2Cu_{3.23(1)}Te_5$, respectively, as summarized in Tables 1 and 2, both with respect to the Te split sites as well as the Cu deficiencies.

Next, a single crystal from the "$Ba_2Cu_{3.3}Se_{0.8}Te_{4.2}$" sample, crystal IV, was mounted on the Bruker Smart APEX. The data

(24) Tsinde, B. P. F.; Doert, T. *Solid State Sci.* **2005**, *7*, 573–587.
(25) Assoud, A.; Soheilnia, N.; Kleinke, H. *Chem. Mater.* **2005**, *17*, 2255–2261.
(26) Lee, C.-S.; Kleinke, K. M.; Kleinke, H. *Solid State Sci.* **2005**, *7*, 1049–1054.
(27) *SAINT*, Version 4; Siemens Analytical X-ray Instruments Inc.: Madison, WI, 1995.
(28) Sheldrick, G. M. *SHELXTL*, Version 5.12; Siemens Analytical X-Ray Systems: Madison, WI, 1995.
(29) Spek, A. L. *J. Appl. Crystallogr.* **2003**, *36*, 7–13.

Table 2. Atomic coordinates, equivalent isotropic displacement parameters and occupancy factors of $Ba_2Cu_{3.33}Te_5$

atom	site	x	y	z	$U_{eq}/Å^2$	occ.	occ.[a]	occ.[b]
Ba	8*f*	0.22033(4)	0.42910(4)	0.16159(3)	0.0227(1)	1	1	1
Cu1	8*f*	0.0626(1)	0.0814(1)	0.07687(9)	0.0249(3)	0.692(3)	0.667(3)	0.677(3)
Cu2	8*f*	0.14105(9)	0.28804(8)	0.42173(6)	0.0249(2)	0.974(3)	0.956(3)	0.944(3)
Te1A	8*f*	0.0747(1)	0.2043(2)	0.59244(7)	0.0174(2)	0.709(5)	0.712(5)	0.716(6)
Te1B	8*f*	0.0936(3)	0.1669(3)	0.5920(2)	0.0174(2)	0.291	0.288	0.284
Te2A	8*f*	0.3490(4)	0.0704(3)	0.1040(2)	0.0175(3)	0.67(1)	0.70(1)	0.73(2)
Te2B	8*f*	0.3209(5)	0.0549(5)	0.1022(4)	0.0175(3)	0.33	0.30	0.27
Te3	4*e*	0	0.17138(5)	0.25	0.0152(1)	1	1	1

[a] Occupancies of $Ba_2Cu_{3.25}Te_5$. [b] Occupancies of $Ba_2Cu_{3.24}Te_5$.

Table 3. Crystallographic Data for $Ba_2Cu_{4-x}(Se,Te)_5$

refined formula	$Ba_2Cu_{3.26(2)}Se_{0.729(8)}Te_{4.271}$, IV	$Ba_2Cu_{3.19(1)}Se_{0.288(7)}Te_{4.712}$, V	$Ba_2Cu_{3.230(8)}Se_{0.130(5)}Te_{4.870}$, VI
formula weight [g/mol]	1084.3	1101.4	1111.47
T of measurement [K]	298(2)	298(2)	298(2)
λ [Å]	0.71073	0.71073	0.71073
space group	$P4_12_12$	$P4_12_12$	$P4_12_12$
a [Å]	6.5418(3)	6.6049(7)	6.6263(5)
c [Å]	25.782(2)	26.026(3)	26.045(2)
V [Å^3]	1103.3(1)	1135.4(2)	1143.6(2)
Z	4	4	4
μ [mm^{-1}]	26.61	25.43	25.22
ρ_{calcd} [g/cm^3]	6.53	6.44	6.46
$R(F_o)^a\backslash R_w(F_o^2)^b$	0.028\0.057	0.025\0.045	0.024\0.036

[a] $R(F_o) = \sum||F_o| - |F_c||/\sum|F_o|$. [b] $R_w(F_o^2) = [\sum w(F_o^2 - F_c^2)^2/\sum w(F_o^2)^2]^{1/2}$.

Table 4. Atomic Coordinates, Equivalent Isotropic Displacement Parameters and Occupancy Factors of $Ba_2Cu_{3.26}Se_{0.73}Te_{4.27}$

atom	site	x	y	z	$U_{eq}/Å^2$	occ.	occ.[a]	occ.[b]
Ba1	8*b*	0.36090(7)	0.14091(7)	0.29278(2)	0.0256(1)	1	1	1
Cu1	8*b*	0.1271(2)	0.3421(2)	0.08386(5)	0.0261(4)	0.742(4)	0.725(3)	0.733(2)
Cu2	8*b*	0.3723(2)	0.4409(2)	0.16775(4)	0.0270(3)	0.887(4)	0.870(3)	0.882(2)
Te1A	8*b*	0.0925(6)	0.1414(3)	0.17021(6)	0.0177(3)	0.72(1)	0.73(1)	0.724(9)
Te1B	8*b*	0.1436(7)	0.1290(7)	0.1691(2)	0.0177(3)	0.28	0.27	0.276
Te2A	8*b*	0.3623(2)	0.1312(7)	0.42619(4)	0.0209(3)	0.92(2)	0.79(4)	0.69(2)
Te2B	8*b*	0.356(2)	0.078(5)	0.4246(5)	0.0209(3)	0.08	0.21	0.31
Se3	4*a*	0.14439(8)	x	0	0.0177(2)	0.729(8) Se, 0.271 Te	0.288(7) Se, 0.712 Te	0.130(5) Se, 0.870 Te

[a] Occupancies of $Ba_2Cu_{3.19}Se_{0.29}Te_{4.71}$. [b] Occupancies of $Ba_2Cu_{3.23}Se_{0.13}Te_{4.87}$.

were collected as described for the ternary case. The unit cell dimensions were indicative of the tetragonal primitive Bravais lattice, and the systematic absences were in accord with the space groups $P4_12_12$ and $P4_32_12$. The structure solution in the former resulted in six atomic positions, tentatively assigned to be one Ba, two Cu, one Se, and two Te atoms. As above-mentioned in case of $Ba_2Cu_{3.3}Te_5$, the two Cu sites exhibited enlarged and the Te atoms significantly anisotropic thermal displacement parameters. Therefore, the Cu site occupancies were refined, and split sites for the Te sites were introduced. Then, the refinement converged with R1 = 0.034 (all data), but the Se site's thermal displacement parameter was only half of the others. Thus, that position was refined as being mixed occupied by Se and Te, resulting in an improved R1 = 0.028 (all data) and an occupancy of 73% Se and 27% Te, corresponding to the refined formula $Ba_2Cu_{3.26(2)}Se_{0.729(8)}Te_{4.271}$. The small Flack parameter of 0.11(5) indicated that the correct absolute conformation was found. As in the case of the ternary telluride, neither super cell reflections nor evidence for twinning were observed. Finally, the parameters were standardized as for the telluride.

To probe the phase range, two more crystals, V and VI, were analyzed via the Bruker Smart APEX, taken from the sample with the intermediate Se content (V, nominal composition: $Ba_2Cu_{3.3}Se_{0.25}Te_{4.75}$) as well as the smallest Se content (VI, nominal composition: $Ba_2Cu_{3.3}Se_{0.10}Te_{4.90}$). The unit cell parameters were significantly larger, indicating a smaller Se concentration, and the systematic absences pointed to the same space group, $P4_12_12$, in both cases. For crystal V, a refinement commencing from the final solution of $Ba_2Cu_{3.26}Se_{0.73}Te_{4.27}$ converged with R1 = 0.025 (all data), a Flack parameter of 0.00(7), and a refined formula of $Ba_2Cu_{3.19(1)}Se_{0.288(7)}Te_{4.712}$. The corresponding data of crystal VI were R1 = 0.024 (all data), a Flack parameter of 0.04(7), and a formula of $Ba_2Cu_{3.230(8)}Se_{0.130(5)}Te_{4.870}$. The crystallographic data of the selenide-telluride are summarized in Table 3, and the atomic parameters including the occupancy factors are given in Table 4.

To summarize, the phase range with respect to Cu is very small, the selenide-telluride adopts a different structure type, and the Se:Te ratio may vary substantially, with $0.13 \le y \le 1.0$ for $Ba_2Cu_{4-x}Se_yTe_{5-y}$.

Calculation of the Electronic Structure. The LMTO (linear muffin tin orbitals) method was employed with the atomic spheres approximation (ASA) for the electronic structure calculations.[30,31] Therein, density functional theory is applied with the local density approximation (LDA) to treat exchange and correlation effects.[32] The following wave functions were used: for Ba 6s, 6p (downfolded[33]), 5d, and 4f; for Cu 4s, 4p, and 3d; for Se 4s, 4p, and 4d (downfolded); and for Te 5s, 5p, and 5d and 4f (the latter two downfolded). The structural parameters were derived from the refinements II ($Ba_2Cu_{3.25}Te_5$) and IV ($Ba_2Cu_{3.26}Se_{0.73}Te_{4.27}$). Two different models were calculated

(30) Andersen, O. K. *Phys. Rev. B* **1975**, *12*, 3060–3083.
(31) Skriver, H. L. *The LMTO Method*; Springer: Berlin, Germany, 1984.
(32) Hedin, L.; Lundqvist, B. I. *J. Phys. C* **1971**, *4*, 2064–2083.
(33) Lambrecht, W. R. L.; Andersen, O. K. *Phys. Rev. B* **1986**, *34*, 2439–2449.

for each of these two compounds because of the Te split sites: one with the majority sites filled, Te1A and Te2A, and the second with the Te1B and Te2B sites. All Cu sites were treated as fully occupied, and the mixed Se/Te position (refined as 73% Se and 27% Te) as a Se site. Therefore, the models retained the full symmetry, and the formulas $Ba_2Cu_4Te_5$ (in space group $C2/c$) and $Ba_2Cu_4SeTe_4$ (in $P4_12_12$).

For $Ba_2Cu_4Te_5$, the eigenvalue problem was solved on the basis of 172 k points of the irreducible wedge of the first Brillouin zone, chosen via the improved tetrahedron method.[34] In case of $Ba_2Cu_4SeTe_4$, 474 k points were selected. To gain insight into the strength of various interactions, crystal orbital Hamilton populations[35] were calculated in addition to the band structures and densities of states.

Physical Property Measurements. In case of the ternary telluride, a cold-pressed bar of the dimensions $6 \times 1 \times 1$ mm of the sample $Ba_2Cu_{3.3}Te_5$ was prepared. The Seebeck coefficient, S, was determined via the SB100 from MMR Technologies between 300 and 550 K, and the electrical resistivity, ρ, via a four-point-method using a homemade device between 300 and 550 K. Silver paint (Ted Pella) was used for the electric contacts in both cases, and both measurements were carried out under dynamic vacuum.

For the selenide-tellurides, larger pellets ($13 \times 2 \times 2$ mm) of $Ba_2Cu_{3.3}Se_yTe_{5-y}$ (with $y = 0.8$ and 1.0) were cold-pressed and then measured utilizing the ULVAC-RIKO ZEM-3 between 300 and 600 K. Therein, S and ρ were simultaneously determined in a helium atmosphere.

Results and Discussion

Crystal Structures. While adopting different structure types, the crystal structures of $Ba_2Cu_{4-x}Te_5$ and $Ba_2Cu_{4-x}(Se,Te)_5$ are all composed of chains of edge-sharing CuQ_4 tetrahedra (with Q = Se, Te), wherein the Cu atoms form cis/trans chains, and the Ba atoms are 9-fold coordinated by the Q atoms (with Q = Se, Te). The $CuTe_4$ chains are connected via interchain Te1−Te2 interactions to puckered layers, which in turn are connected via common $Q3$ atoms to a three-dimensional Cu−Q network. The crystal structure of $Ba_2Cu_{4-x}Te_5$ is depicted in Figure 1, with the Ba−Te bonds being omitted for clarity.

The different symmetry of the selenide-telluride, compared to the telluride, reflects itself in a different orientation of these layers along the crystallographic c axis, which is twice as long in case of the selenide-telluride. The a and b axes are all around 6.6 Å for the selenide-telluride and for the telluride in the primitive setting as well. In both cases, the interconnection along c occurs via the Ba−Q bonds as well as corner-sharing of the CuQ_4 tetrahedra. The layers all run parallel to the a,b plane, and are packed along c according to ABAB··· in case of the telluride and ABCDABCD··· in case of the selenide-telluride (Figure 2).

A striking feature of these two structure types is the occurrence of almost linear Te atom chains (which do not show any Se incorporation), depicted via the dashed lines in Figures 1 and 2. Therein, the Te−Te distances alternate between shorter contacts of the order of 3.0 Å and longer ones of about 3.6 Å (Figure 3). Because the chains consist of the split sites of Te1 and Te2, various Te−Te distances may occur, depending on which split site is filled. For example in $Ba_2Cu_{3.19}Se_{0.29}Te_{4.71}$, the Te1A−Te2A distances are 3.03 Å and 3.58 Å, and the Te1B−Te2B 2.97 Å and 3.65 Å. The distances are almost equal in a Te1A/Te2B chain fragment with 3.32 Å and 3.28 Å, and in case of Te1B/Te2A, the separation is intermediate with 3.22 Å and 3.40 Å (Tables 5, 6).

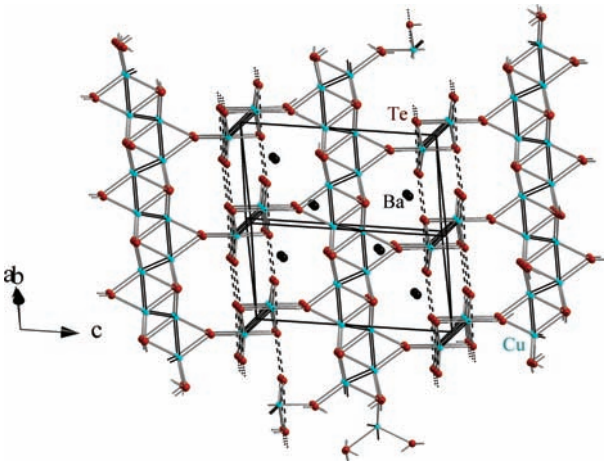

Figure 1. Crystal structure of $Ba_2Cu_{4-x}Te_5$. Ba−Te bonds are omitted for clarity.

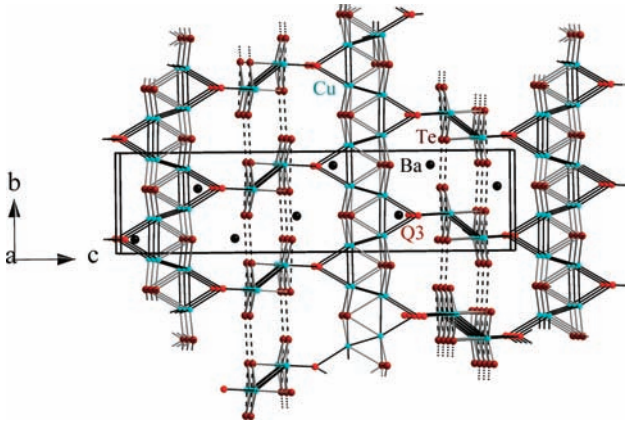

Figure 2. Crystal structure of $Ba_2Cu_{4-x}(Se,Te)_5$. Ba−Se and Ba−Te bonds are omitted for clarity.

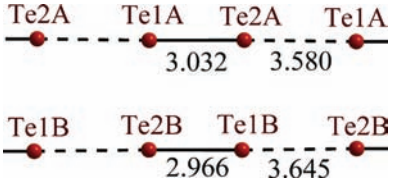

Figure 3. Various Te atom chains of $Ba_2Cu_{3.19}Se_{0.29}Te_{4.71}$.

The shortest of these distances resemble hypervalent (half) Te−Te bonds, as, for example, found in the square nets of $LaSeTe_2$ (3.05 Å),[36] the square planar Te_5^{6-} units of K_2SnTe_5 (3.02 Å and 3.05 Å)[37] or the linear center of the Te_5^{4-} fragment of Ba_2SnTe_5 (3.02 Å and 3.10 Å)[38] or

(34) Blöchl, P. E.; Jepsen, O.; Andersen, O. K. *Phys. Rev. B* **1994**, *49*, 16223–16233.
(35) Dronskowski, R.; Blöchl, P. E. *J. Phys. Chem.* **1993**, *97*, 8617–8624.
(36) Doert, T.; Fokwa, B. P. T.; Simon, P.; Lidin, S.; Söhnel, T. *Chem.—Eur. J.* **2003**, *9*, 5865–5872.
(37) Bernstein, J.; Hoffmann, R. *Inorg. Chem.* **1985**, *24*, 4100–4108.
(38) Assoud, A.; Derakhshan, S.; Soheilnia, N.; Kleinke, H. *Chem. Mater.* **2004**, *16*, 4193–4198.

Table 5. Selected Interatomic Distances [Å] of $Ba_3Cu_{4-x}Te_5$

interaction	d/Å[a]	d/Å[b]	d/Å[c]
Ba−Te1A/B	3.669(1)/3.511(3)	3.6705(2)/3.512(3)	3.674(1)/3.524(3)
Ba−Te1A/B	3.742(2)/4.017(3)	3.734(2)/4.007(3)	3.741(2)/4.003(4)
Ba−Te1A/B	3.863(3)/3.936(4)	3.849(2)/3.922(3)	3.845(2)/3.923(3)
Ba−Te2A/B	3.460(3)/3.451(6)	3.458(2)/3.445(5)	3.463(2)/3.454(6)
Ba−Te2A/B	3.569(3)/3.455(6)	3.565(3)/3.459(5)	3.563(3)/3.458(6)
Ba−Te2A/B	3.690(3)/3.888(5)	3.686(3)/3.885(5)	3.699(2)/3.888(5)
Ba−Te2A/B	3.703(2)/3.755(5)	3.694(2)/3.737(5)	3.695(4)/3.746(6)
Ba−Te3	3.5040(6)	3.4942(5)	3.4971(5)
Ba−Te3	3.5425(6)	3.5330(5)	3.5339(5)
Cu1−Te1A/B	2.627(2)/2.555(3)	2.620(2)/2.550(3)	2.621(2)/2.551(3)
Cu1−Te1A/B	2.682(2)/2.345(3)	2.675(2)/2.342(3)	2.680(2)/2.359(4)
Cu1−Te2A/B	2.665(4)/2.414(5)	2.655(4)/2.405(5)	2.651(5)/2.414(6)
Cu1−Te3	2.630(1)	2.624(1)	2.623(1)
Cu1−Cu1	2.632(2)	2.634(2)	2.642(2)
Cu1−Cu2	2.734(1)	2.717(1)	2.712(1)
Cu2−Te1A/B	2.597(1)/2.651(3)	2.593(1)/2.647(3)	2.598(1)/2.641(3)
Cu2−Te1A/B	2.738(2)/2.591(3)	2.732(1)/2.586(3)	2.732(2)/2.583(3)
Cu2−Te2A/B	2.669(3)/2.552(5)	2.659(3)/2.553(5)	2.660(3)/2.553(6)
Cu2−Te3	2.6382(9)	2.6308(8)	2.6317(9)
Cu2−Cu1	2.734(1)	2.717(1)	2.712(1)
Cu2−Cu2	2.713(2)	2.715(2)	2.717(2)
Te1A−Te2A/B	3.028(5)/3.316(5)	3.027(5)/3.248(5)	3.038(6)/3.307(7)
Te1A−Te2A/B	3.636(4)/3.349(5)	3.618(4)/3.309(5)	3.610(4)/3.316(5)
Te1B−Te2A/B	3.264(4)/2.974(6)	3.248(4)/2.964(6)	3.247(5)/2.976(8)
Te1B−Te2A/B	3.404(4)/3.689(4)	3.399(4)/3.679(6)	3.403(5)/3.670(7)

[a] $Ba_2Cu_{3.33}Te_5$. [b] $Ba_2Cu_{3.25}Te_5$. [c] $Ba_2Cu_{3.24}Te_5$.

Table 6. Selected Interatomic Distances [Å] of $Ba_3Cu_{4-x}(Se,Te)_5$

interaction	d/Å[a]	d/Å[b]	d/Å[c]
Ba1−Te1A/B	3.615(2)/3.497(5)	3.643(2)/3.520(4)	3.649(2)/3.532(4)
Ba1−Te1A/B	3.721(2)/3.945(5)	3.763(2)/3.980(5)	3.771(3)/3.984(4)
Ba1−Te1A/B	3.747(2)/3.834(5)	3.771(2)/3.904(5)	3.779(3)/3.912(4)
Ba1−Te2A/B	3.440(1)/3.43(1)	3.468(2)/3.433(8)	3.468(3)/3.442(6)
Ba1−Te2A/B	3.488(2)/3.36(2)	3.540(4)/3.461(9)	3.560(4)/3.461(6)
Ba1−Te2A/B	3.675(2)/3.87(2)	3.694(4)/3.85(1)	3.690(4)/3.840(7)
Ba1−Te2A/B	3.691(2)/3.82(2)	3.699(4)/3.77(1)	3.696(4)/3.790(7)
Ba1−*Q*3	3.4305(7)	3.4716(6)	3.4883(5)
Ba1−*Q*3	3.4735(7)	3.5112(6)	3.5223(5)
Cu1−Te1A/B	2.594(2)/2.604(5)	2.560(2)/2.586(4)	2.603(2)/2.586(5)
Cu1−Te1A/B	2.685(3)/2.404(5)	2.694(3)/2.417(5)	2.701(3)/2.428(5)
Cu1−Te2A/B	2.581(3)/2.39(2)	2.634(7)/2.43(1)	2.652(5)/2.451(7)
Cu1−*Q*3	2.522(1)	2.596(1)	2.6168(9)
Cu1−Cu2	2.625(2)	2.670(1)	2.694(1)
Cu1−Cu2	2.769(2)	2.712(1)	2.694(1)
Cu2−Te1A/B	2.630(2)/2.557(5)	2.625(2)/2.558(4)	2.625(2)/2.556(4)
Cu2−Te1A/B	2.682(3)/2.530(5)	2.704(3)/2.509(5)	2.713(2)/2.519(5)
Cu2−Te2A/B	2.617(4)/2.37(2)	2.651(5)/2.53(1)	2.672(5)/2.523(7)
Cu2−*Q*3	2.506(1)	2.5827(9)	2.6039(8)
Cu2−Cu1	2.625(2)	2.670(1)	2.694(1)
Cu2−Cu1	2.769(2)	2.712(1)	2.694(1)
Te1A−Te2A/B	3.021(6)/3.18(3)	3.032(9)/3.32(1)	3.016(7)/3.284(8)
Te1A−Te2A/B	3.528(6)/3.37(3)	3.580(9)/3.28(1)	3.617(5)/3.346(7)
Te1B−Te2A/B	3.196(7)/2.85(3)	3.22(1)/2.97(1)	3.262(8)/2.990(7)
Te1B−Te2A/B	3.358(6)/3.70(3)	3.40(1)/3.65(1)	3.377(5)/3.644(8)

[a] $Ba_2Cu_{3.26}Se_{0.73}Te_{4.27}$. [b] $Ba_2Cu_{3.19}Se_{0.29}Te_{4.71}$. [c] $Ba_2Cu_{3.23}Se_{0.13}Te_{4.87}$.

NaTe (2× 3.08 Å).[39] Treating these contacts as such half bonds and the longer ones as nonbonding, the chains may

(39) Böttcher, P.; Keller, R. *J. Less-Common Met.* **1985**, *109*, 311–321.

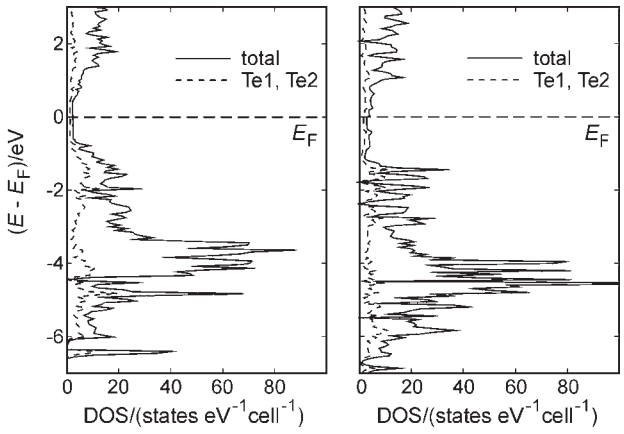

Figure 4. Densities of states (DOS) of the $Ba_2Cu_4Te_5$ models. Left: model A, using Te1A and Te2A; right: model B, using Te1B and Te2B.

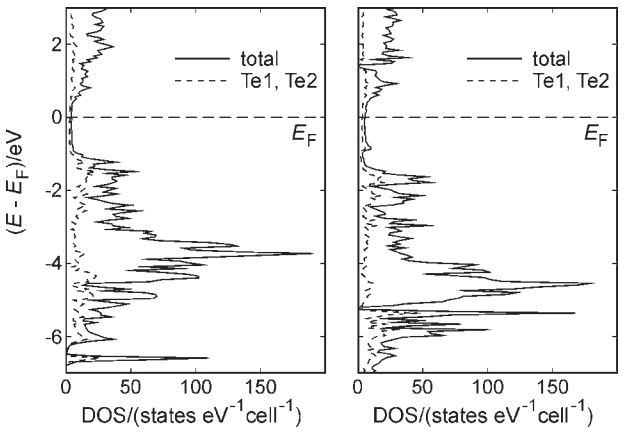

Figure 5. Densities of states (DOS) of the $Ba_2Cu_4SeTe_4$ models. Left: model A, using Te1A and Te2A; right: model B, using Te1B and Te2B.

be described as infinite Te_2^{3-} chains. As the third Q atom, $Q3$, participates in no $Q-Q$ contacts < 3.5 Å, it may be viewed as Q^{2-}. Then, four positive charges remain for the $4 - x$ Cu atoms, according to $(Ba^{2+})_2Cu_{4-x}{}^{4+}Q^{2-}(Te_2{}^{3-})_2$.

This third $Q3$ site is the preferred one for the Se incorporation: at the Se-rich side of the phase range, we found no evidence for any Se contact in the Te1−Te2 chain, and 73% Se and 27% Te on the $Q3$ site. The preference of the Se atom for the site with fewer $Q-Q$ interactions and higher formal charge is a consequence of its higher electronegativity, compared to Te, and was also observed in the structure of $LaSeTe_2$.[36] Because of its smaller size, the Ba−$Q3$ and Cu−$Q3$ distances decrease with increasing Se content, as does the unit cell volume. For example, while all Cu−Te3 bonds in the ternary tellurides are between 2.62 Å and 2.64 Å, the corresponding distances are 2.62 Å (Cu1−$Q3$) and 2.60 Å (Cu2−$Q3$) for the case with 13% Se on $Q3$, 2.60 Å (Cu1−$Q3$) and 2.58 Å (Cu2−$Q3$) for 29% Se case, and 2.52 Å (Cu1−$Q3$) and 2.51 Å (Cu2−$Q3$) for the 73% Se case. Likewise, the unit cell volume decreases from 1151 Å^3, averaged over the three telluride data sets, to 1144 Å^3 for $Ba_2Cu_{3.23}Se_{0.13}Te_{4.87}$ and 1135 Å^3 for $Ba_2Cu_{3.19}Se_{0.29}Te_{4.71}$ and 1103 Å^3 for $Ba_2Cu_{3.26}Se_{0.73}Te_{4.27}$. The same trend was found for $Ba_3Cu_{17-x}(Se,Te)_{11}$.[9]

The Cu atom chains exhibit Cu−Cu distances between 2.62 Å and 2.73 Å, depending on the Se content. These numbers compare well to the distances in Ba_3Cu_{17-x}(Se,

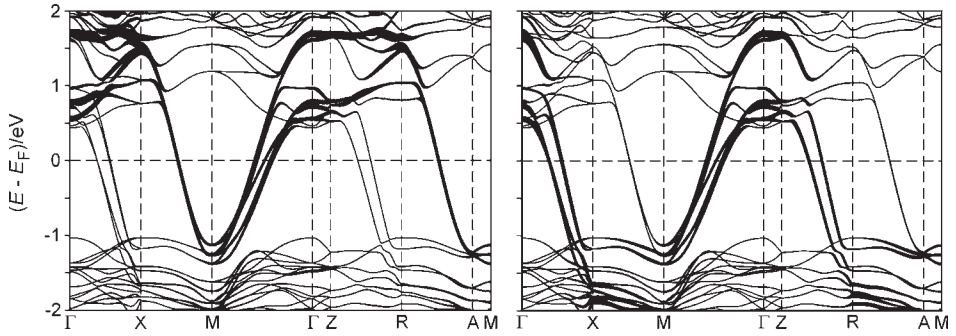

Figure 6. Band structure of the $Ba_2Cu_4SeTe_4$ model A. Left: emphasis of the p_x contributions of Te1A and Te2A; right: p_y. Γ: (0, 0, 0); X: (0, 0.5, 0); M: (0.5, 0.5, 0); Z: (0, 0, 0.5); R: (0, 0.5, 0.5); A: (0.5, 0.5, 0.5), in fractional coordinates of the reciprocal lattice.

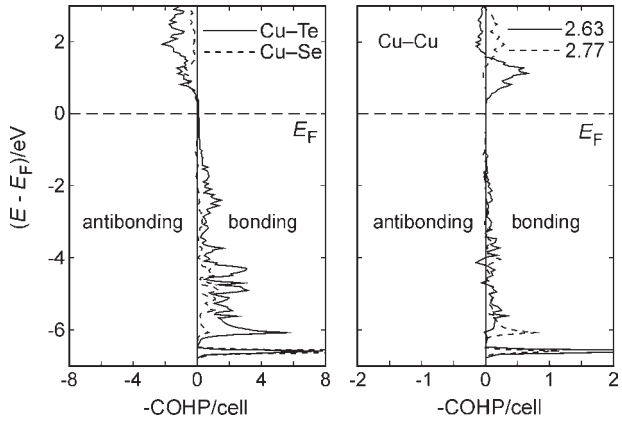

Figure 7. Selected cumulated crystal orbital Hamilton population (COHP) curves of the $Ba_2Cu_4SeTe_4$ model A. Left: Cu−*Q*; right: Cu−Cu.

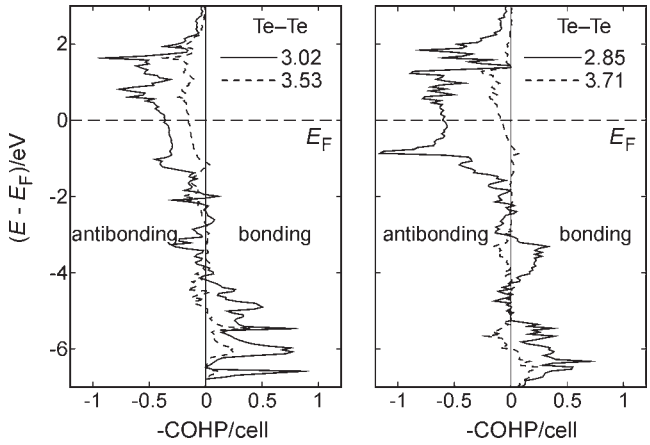

Figure 8. Te−Te crystal orbital Hamilton population (COHP) curves of the $Ba_2Cu_4SeTe_4$ models A (left) and B (right).

Te)$_{11}$[9] and in $Ba_3Cu_{14-x}Te_{12}$.[6] Interactions of these lengths are common in Cu^+ chalcogenides, and their bonding character, despite a formal $d^{10}s^0p^0$ configuration of Cu^+, is generally understood based on hybridization effects,[40−42] as further discussed below.

Another typical observation is the significant Cu deficiency in Cu chalcogenides. In this case, a connection of the Cu deficiency with the Te split site is apparent because of the too short Cu1−Te1B and Cu1−Te2B distances. For example in $Ba_2Cu_{3.33}Te_5$, the distances are 2.35 Å and 2.41 Å, respectively, significantly shorter than the regular Cu−Te distances of 2.6 Å−2.7 Å, and the occupancies were refined to 74% for Cu1 (i.e., a deficiency of 26%), 28% for Te1B, and 8% for Te2B. One may thus assume that the Cu deficiency causes the Te split sites, that is, the ideal position of these Te atoms depends on whether or not a neighboring Cu1 atom is present.

Electronic Structures. The densities of states, DOS, of the two $Ba_2Cu_4Te_5$ models A (based on Te1A and Te2A) and B (based on Te1B and Te2B) are compared in Figure 4. In both cases, a distinct pseudo band gap appears at the Fermi level, E_F, where the states are dominated by the Te1 and Te2 contributions. The Cu 3d states dominate the area between −2 and −5 eV.

The densities of states of two $Ba_2Cu_4SeTe_4$ models show very similar features, for example, the pseudo gap and the Cu d peaks (Figure 5). The absence of a band gap in the vicinity of E_F distinguishes these materials from the other Ba−Cu chalcogenides studied by us so far: $Ba_3Cu_{14-x}Te_{12}$,[6] $Ba_{6.76}Cu_{2.42}Te_{14}$,[7] $Ba_2(Cu,Ag)_4Se_5$,[8] $Ba(Cu,Ag)_2Te_2$,[43] and $Ba_3Cu_{17-x}(Se,Te)_{11}$[9] all exhibit such gaps and are *p*-type semiconductors.

The p_x and p_y contributions of the Te atoms of the quasi-linear Te chains, that run parallel to both the *a* and the *b* axis of the selenide-telluride, cause the absence of the energy gap, as demonstrated via the fat band[44] representation (Figure 6). The bands originating from these orbitals cross E_F in the *a**, *b** plane with large dispersions, while no bands cross E_F parallel to *c**. Such a scenario is indicative for two-dimensional metallic properties. With the experimentally observed Cu deficiency of $x \approx 0.75$, one can approximate that the actual electron count is 0.75 electrons less per formula unit, when Cu is in its +1 state. This would lower the Fermi level by 0.7 eV in the case of the telluride as well as selenide-telluride, that is, into an area that is still dominated by the steep bands of the p_x and p_y contributions of the Te atoms of the quasi-linear Te chains.

The crystal orbital Hamilton population curves computed for model A of $Ba_2Cu_4SeTe_4$ demonstrate that no Cu−*Q* or Cu−Cu bonds contribute to the states around E_F (Figure 7). Both the Cu−Se and Cu−Te bonds are optimized, as the Fermi level separates the filled bonding from the empty antibonding states. Most of the strength

(40) Mehrotra, P. K.; Hoffmann, R. *Inorg. Chem.* **1978**, *17*, 2187–2189.
(41) Merz, K. M., Jr.; Hoffmann, R. *Inorg. Chem.* **1988**, *27*, 2120–2127.
(42) Pyykkö, P. *Chem. Rev.* **1997**, *97*, 597–636.
(43) Assoud, A.; Cui, Y.; Thomas, S.; Sutherland, B.; Kleinke, H. *J. Solid State Chem.* **2008**, *181*, 2024–2030.
(44) Jepsen, O.; Andersen, O. K. *Z. Phys.* **1995**, *97*, 35–47.

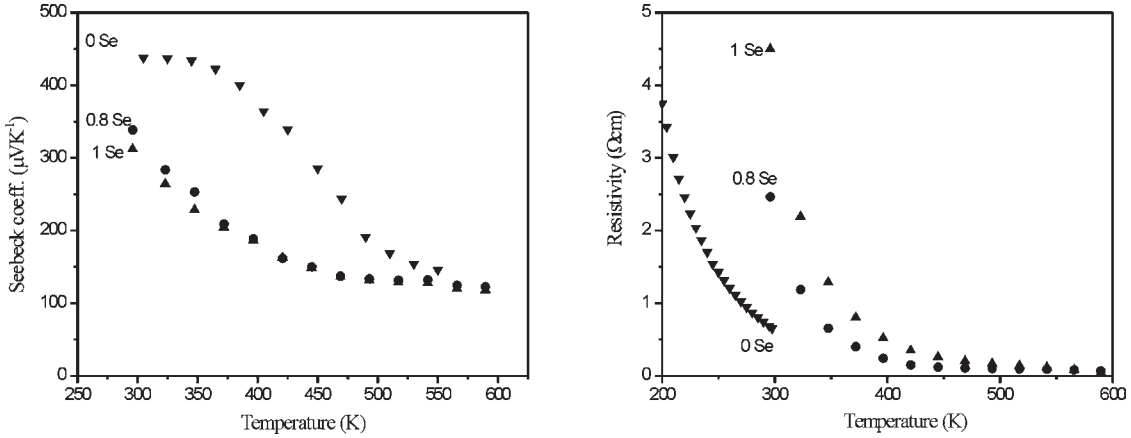

Figure 9. Seebeck coefficient (left) and electrical resistivity (right) of $Ba_2Cu_{3.3}Se_yTe_{5-y}$.

of the Cu−Cu bonds comes from the strongly bonding peak at −6.5 eV, which also occurs within the Cu−*Q* interactions. The largest contribution to this peak comes from the p_z orbitals of Se3, covalently mixing with the s orbitals of both Cu sites. This in turn explains why Cu−Cu bonding occurs despite the normally assumed d^{10} configuration. While the Cu−Cu bonds also exhibit basically no states at E_F and almost exclusively bonding states below E_F, the states in the region up to 1.5 eV above E_F are bonding as well. Hence, an increase in the valence electron concentration would occur with weakened Cu−*Q*, but strengthened Cu−Cu interactions, while a decrease, as experimentally observed because of the Cu deficiency, would weaken all these interactions by depopulating bonding states.

On the other hand, both different Te1A−Te2A and both different Te1B−Te2B interactions of $Ba_2Cu_4SeTe_4$ become antibonding well below E_F, and have a significant contribution directly at E_F (Figure 8). Therefore, a smaller valence electron concentration would lead to stronger Te−Te bonds. In the model $Ba_2Cu_4SeTe_4$, the shorter ones of 3.02 Å (Te1A−Te2A) and 2.85 Å (Te1B−Te2B) are significantly bonding with integrated COHP values, ICOHP,[45] of −0.46 and −0.29 eV, respectively. Here, the shorter interaction is the weaker bond, because more antibonding states are filled. The two longer interactions of 3.53 Å and 3.71 Å are basically net nonbonding, with ICOHP values of 0.06 and −0.01 eV.

Physical Properties. Although the band structure calculations pointed toward two-dimensional metallic character, $Ba_2Cu_{3.3}Se_yTe_{5-y}$ with $y = 0$, 0.8, 1.0 were all determined to be *p*-type semiconductors with large Seebeck coefficient values, *S*. *S* decreases with increasing Se content, for example, at 300 K from $+440\ \mu V\ K^{-1}$ for $y = 0$ to $+340\ \mu V\ K^{-1}$ for $y = 0.8$ and to $+310\ \mu V\ K^{-1}$ for $y = 1.0$. In all three cases, *S* decreases with increasing temperature, for example, from 300 to 500 K down to $+170\ \mu V\ K^{-1}$ for $y = 0$ (Figure 9).

The electrical resistivity, ρ, decreases almost exponentially with increasing temperature, as is typical for extrinsic semiconductors. ρ increases with increasing *y* within the series $Ba_2Cu_{3.3}Se_yTe_{5-y}$: at 300 K, the values are 0.65 Ω cm for $y = 0$, 2.5 Ω cm for $y = 0.8$, and 4.5 Ω cm for $y = 1.0$. At 500 K, all values have fallen below 0.2 Ω cm. The increase of ρ with increasing Se concentration is expected for a semiconducting selenide-telluride, for the band gap increases with increasing Se because of its higher electronegativity, which lowers the valence band.[46]

Conclusions

Two new structure types were uncovered, one adopted by the telluride $Ba_2Cu_{4-x}Te_5$ and the other by the selenide-telluride $Ba_2Cu_{4-x}Se_yTe_{5-y}$. Therein, *x* may vary at least within $0.67 \le x \le 0.81$, and *y* within $0.13 \le y \le 1.0$. Both structures are composed of the same structure motifs, but exhibit a different long-range order. The structures include unusual Te atom chains with alternating short distances of the order of 3.0 Å and long ones of the order of 3.6 Å. The former are bonding, albeit being longer than typical Te−Te single bonds, and the latter are basically nonbonding, because the filled bonding states are matched by the filled antibonding states. Both Cu sites exhibit significant deficiencies in all cases, which appear to be connected to the split sites of the two independent Te atoms of the Te atom chains.

The fact that these materials are semiconductors, as experimentally determined, in contrast to the calculated band structures, implies that the models chosen for the calculations were not close enough to the reality, considering the various split sites combined with the Cu atom deficiencies. The calculated band structures indicated two-dimensional metallic properties caused by the Te−Te interactions, which should be prone to undergo a Peierls distortion.

Acknowledgment. Financial support from NSERC, CFI, OIT (Ontario Distinguished Researcher Award for H.K.), and the Canada Research Chair program (CRC for H.K.) is appreciated. Acknowledgment is also made to the Donors of the American Chemical Society Petroleum Research Fund for partial support of this research.

Supporting Information Available: Six crystallographic information files (CIFs), and DSC plots of $Ba_2Cu_{3.3}Te_5$ and $Ba_2Cu_{3.3}Se_{0.8}Te_{4.2}$. This material is available free of charge via the Internet at http://pubs.acs.org.

(45) Landrum, G. A.; Dronskowski, R. *Angew. Chem., Int. Ed.* **2000**, *39*, 1560–1585.

(46) Assoud, A.; Soheilnia, N.; Kleinke, H. *Z. Naturforsch.* **2004**, *59b*, 975–979.